Smart Structures and Systems, *Vol. 36, No. 3 (2025) 157-166*
https://doi.org/10.12989/sss.2025.36.3.157

UAV inspection-based aftershock fragility analysis of deteriorated PSC bridge structure considering mainshock-aftershock sequences

Sangmok Lee [1a] and Sungsik Yoon*[2]

[1] *Dam Safety Management Center, Korea Water Resources Corporation (K-water), 200 Sintanjin-ro, Daedeok-gu, Daejeon 34350, Republic of Korea*
[2] *Department of Artificial Intelligence, Hannam University, 70 Hannam-ro, Daedeok-gu, Daejeon 34430, Republic of Korea*

(*Received April 22, 2025, Revised August 23, 2025, Accepted September 2, 2025*)

Abstract. Past earthquake events show that aftershocks may arise within a short interval following a mainshock. Structural deformation caused by a mainshock can affect structural responses during an aftershock. Therefore, this study explores the aftershock fragility analysis of a bridge structure considering mainshock-aftershock sequential ground motions, and the result of sequential ground motion is compared with that of aftershock ground motion. In the numerical example, an in-service pre-stressed concrete (PSC) bridge that was constructed more than forty years ago is selected as the target structure. To consider structural deterioration of the bridge, a recently proposed approach based on unmanned aerial vehicle (UAV) damage detection is introduced. In the approach, the percent reduction in elastic modulus is computed in accordance with the selected damage states. To derive aftershock fragility curves, nonlinear time-history analyses are conducted using ten sets of mainshock-aftershock sequential ground motions, and the analyses are also conducted using the single aftershock ground motions for comparison. The result shows that the failure probability of the target structure increased due to the mainshock effect.

Keywords: aftershock fragility; failure probability; mainshock-aftershock sequence; PSC bridge; UAV inspection

1. Introduction

Earthquakes are a natural disaster that can cause severe structural damage. A mainshock is the largest earthquake in a sequence and is commonly followed by many aftershocks. For example, according to the Korea Meteorological Administration report (KMA 2017), the 2016 Gyeongju earthquake of magnitude 5.8 occurred in the Korea Peninsula and resulted in 554 aftershocks of magnitude 1.5 or more by the end of the year (Yoon *et al*. 2020a, b). In addition, there is growing interest in research on detecting damage to structures caused by external loads (Onat and Gul 2018, Akin and Sahin 2017, Hakim and Razak 2014, Peng-hui *et al*. 2015). The frequent observation of sequential earthquake events and the importance of damage detection highly motivated this study to conduct seismic fragility analysis of a deteriorated structure considering mainshock-aftershock sequences (Yoon *et al*. 2018).

Seismic fragility analysis of a structure yields probabilities of exceeding given limit states with varying earthquake ground motion intensities. The results are commonly expressed by seismic fragility curves. To derive seismic fragility curves, a simple mathematical form of the standard normal cumulative distribution function, which is known as a fragility function, is widely used (Choi *et al*. 2004, Nielson and DesRoches 2007, Rajeev and Tesfamariam 2012, Zhang and Zirakian 2015, Lee *et al*. 2019, Yoon *et al*. 2021a). In the function, structural capacity and demand are modeled assuming that they are lognormally distributed. The main purpose of this study is to evaluate the lognormal distribution parameters of structural capacity and demand. A probabilistic seismic demand model (PSDM) is utilized to determine the lognormal distribution parameters (Mackie and Stojadinović 2005).

Earthquake engineering communities have been interested in the effect of mainshock-aftershock sequences on seismic fragility of structures, and many studies have been conducted to investigate structural responses considering mainshock-aftershock sequences for various types of structures. Pang *et al*. (2019) studied the seismic performance of a concrete-faced rockfill dam subjected to mainshock-aftershock sequences. The result presented that the seismic sequence caused larger deformation compared to single aftershocks. In the study of Zhang *et al*. (2021), the nonlinear time-history analysis of unreinforced and confined masonry structures was performed under mainshock-aftershock sequences and single aftershocks of the same intensities, respectively. As a result, the mainshock-damaged models notably increased the roof displacement compared with the single aftershock-damaged models. Li *et al*. (2014a) explored the aftershock collapse probability of a mainshock-damaged four-story steel building. The study showed that the structural collapse capacity can be remarkably reduced when the building is affected by a high intensity mainshock. In addition, the building is vulnerable to collapse in a low intensity

*Corresponding author, Ph.D., Assistant Professor,
E-mail: sungsik@hnu.kr
[a] Ph.D., P.E.

ISSN: 1738-1584 (Print), 1738-1991 (Online)

aftershock following the mainshock. Omranian *et al*. (2018) focused on comparison of seismic vulnerability assessment of a reinforced concrete (RC) skew bridge considering mainshock-aftershock sequences and mainshock only. The result indicated that aftershocks can significantly affect seismic fragilities. Gaetani d'Aragona *et al*. (2017) derived aftershock collapse fragility curves of a non-ductile RC building conditioned on several return periods of mainshocks. The aftershock fragility increased as the mainshock intensity increased for both non-collapse and collapse states. Therefore, considering a mainshock-aftershock sequence is necessary to estimate the seismic demand under an aftershock.

Regular structure inspection is important because of the decrease in structural capacity due to deterioration over time. For structural maintenance purpose, previous researchers have utilized computer algorithms to predict the responses of structures under various environmental conditions. For example, Onat and Gul (2018) evaluated the out of plane structural response of infill wall structure by employing artificial neural network. Hakim and Razak (2014) and Peng-hui *et al*. (2015) adopted artificial neural network to identify the structural damage and modal parameters. As image processing technologies utilizing computers have advanced, numerous studies have been conducted to detect damage in structures. Yoon *et al*. (2021b) utilized 3D image coordinates to identify the locations of exterior structural damage and to detect missing regions of interest in unmanned aerial vehicle (UAV)-based visual inspections. Moreover, Yoon *et al*. (2022b) proposed a robust methodology that updates the digital twin model of bridge structures employing UAV inspection and evaluated the seismic performance of deteriorated bridge structures based on the updated model. However, the updated model was not utilized to assess the seismic performance under consecutive earthquake events, such as mainshock–aftershock sequences.

To conduct more accurate static or dynamic analysis of deteriorated structures, the material property of the structural components should be updated. However, few studies have addressed mainshock-aftershock fragility while considering the effects of deterioration. To address this gap, the present study implements the recently proposed approach (Yoon *et al*. 2022b) and incorporate it into an aftershock fragility evaluation that accounts for mainshock-aftershock sequences, which is the main emphasis of this study. The approach adopted UAV-based visual inspection and utilizes the region-based convolutional neural network (R-CNN) algorithm to identify structural damage. Subsequently, the damage grade and corresponding damage index are determined to estimate the material property of structural components.

Using the UAV inspection-based method, the FE model is updated to reflect the deterioration of the target bridge, and the updated model is subsequently employed to perform the mainshock-aftershock analysis. To consider the uncertainty of ground motions, ten pairs of mainshock-aftershock sequential ground motions are used. The drift ratio of piers is chosen as the engineering demand parameter, and the probability distribution parameters of seismic demand are calculated based on the results of nonlinear time-history analyses. The capacity limits suggested by Dutta and Mander (1998) are applied to aftershock fragility assessment. Finally, aftershock fragility curves are derived under mainshock-aftershock sequences. The effect of mainshock-aftershock sequences on aftershock fragility is studied through comparison with fragility curves derived from single aftershock.

2. Seismic fragility curve derivation

This study aims to derive seismic fragility curves considering mainshock–aftershock sequential ground motions, with a particular focus on how the mainshock–aftershock sequence influences the aftershock fragility of a structure. Seismic fragility curves provide a probabilistic measure of structural safety against earthquakes by representing the probability of failure at different levels of ground motion intensity. The failure probability (P_f) quantifies the conditional probability of the seismic demand (D) exceeding the capacity (C) for a specified intensity measure (IM), as shown in Eq. (1) (Padgett and DesRoches 2008).

$$P_f = P[D \geq C|IM] \tag{1}$$

To compute failure probabilities with the structural response, nonlinear time-history analysis is conducted using the FE model. This analysis is repeated for different IM values to estimate the structural responses. Subsequently, a PSDM is derived through linear regression of these seismic responses against the corresponding IM values such as Peak Ground Acceleration (PGA), Peak Ground Velocity (PGV), etc. (Mackie and Stojadinović 2005). The PSDM is commonly utilized to generate seismic fragility curves for bridge structures (Nielson and DesRoches 2007, Mangalathu *et al*. 2018). The D is approximated as shown in Eq. (2) (Cornell *et al*. 2002), with parameters a and b of the demand model.

$$D = a \cdot IM^b \tag{2}$$

This equation can be reformulated as a linear equation in the natural logarithmic domain, as described in Eq. (3). Through linear regression analysis, the unknown parameters a and b are determined.

$$\ln(D) = \ln(a) + b \cdot \ln(IM) \tag{3}$$

The logarithmic dispersion of the demand given IM, $\beta_{D|IM}$, is calculated using Eq. (4) (Nielson and DesRoches 2007), where d_i denotes the peak demand values derived from nonlinear time-history analyses, and N is the total number of input ground motions.

$$\beta_{D|IM} \cong \sqrt{\frac{\sum_{i=1}^{N}(\ln(d_i) - \ln(D))^2}{N-2}} \tag{4}$$

Assuming that both demand and capacity follow lognormal distributions, the failure probability defined in Eq. (1) can be reformulated as shown in Eq. (5). Here, S_D and S_C represent the median values of the demand and

capacity, respectively, and β_C refers to the logarithmic dispersion of the capacity, and $\Phi(\cdot)$ is the standard normal cumulative distribution function.

$$P_f = P[D \geq C|IM] = \Phi\left(\frac{\ln(S_D) - \ln(S_C)}{\sqrt{\beta_{D|IM}^2 - \beta_C^2}}\right) \quad (5)$$

3. Numerical example

3.1 Target structure

Deteriorated structures are generally more vulnerable to earthquakes than their original counterparts. Accordingly, this study focuses on the Deungsun Bridge, constructed in the 1980s in South Korea, a period during which seismic design codes were not yet implemented. The bridge has a total span length of 2,000 meters and a width of 11 meters, consisting of 40 spans with a maximum individual span length of 50 meters. The superstructure comprises prestressed concrete (PSC) box girders, and this study designates two of these spans as the region of interest (ROI). These two spans form a segmented deck supported by two girders and three piers. Fig. 1 shows the target bridge, with the ROI indicated with a white rectangle.

To identify the current condition of the bridge, a novel approach recently proposed by Yoon *et al*. (2022b) was adopted. This approach consists of two detailed phases: (1) a UAV-based damage detection phase and (2) a bridge condition assessment phase. In the first phase, a UAV inspection of the ROI is conducted, and a mask R-CNN algorithm is utilized to efficiently detect damage (He *et al*. 2017). The damage of concrete members is classified into six types: cracks, rebar exposure, water leakage, breakage, material segregation, and efflorescence.

Once the damage is detected through deep learning algorithm, the second phase involves assessing the bridge condition. South Korea's five-level damage grading system (Grades A to E) is adopted (Oh *et al*. 2001). In this process, only the external damage identified through UAV inspection is considered for grading. The classification is based on the type of damage (crack and non-crack damage), as specified in South Korean guidelines (MOLIT 2019, 2020). Note that Grades D and E are excluded from this study, as these conditions restrict access to vehicles or pedestrians. The estimated damage grades are then linked to the damage states and damage indices proposed by Shinozuka *et al*. (2003). The damage state of the bridge is categorized into five levels: no damage, minor damage, moderate damage, major damage, and collapse. Table 1 presents the correspondence between damage grades and their associated damage indices.

Fig. 1 Target region of the bridge

Table 1 Damage grade and corresponding damage index

Damage grade (in Korea)	Damage state (Shinozuka *et al*. 2003)	Damage index (Shinozuka *et al*. 2003)
A	No	0
B	Minor	0.1
C	Moderate	0.3
D	Major	0.75
E	Collapse	1.0

3.2 FE model generation

The aim of this study is to evaluate the aftershock fragility of a deteriorated bridge under mainshock–aftershock sequential ground motions, and to compare the results with those obtained using aftershock ground motions only. To develop a FE model of the PSC bridge, which is comprised of a single box girder and RC piers, the software Zeus-NL, specifically designed for nonlinear dynamic analysis (Elnashai *et al*. 2010), was employed. Zeus-NL has been widely used in seismic fragility assessments (Lee and Moon 2014, Moon *et al*. 2018, Lee *et al*. 2021). The numerical model was developed based on the structural drawings of the bridge. A simplified three-dimensional model is shown in Fig. 2.

For the purpose of iterative nonlinear time history analyses, an eccentric beam model was employed (Chan and Chan 1999). This model simplifies the complex behavior of fully composite structures by using beam and truss elements, and represents slabs, girders, and PSC tendons through rigid link elements. The eccentric beam

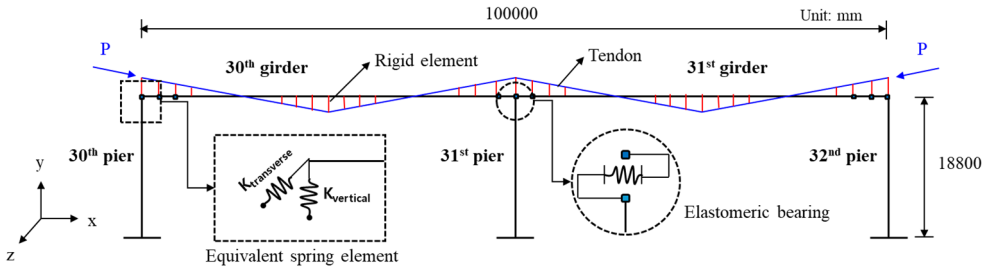

Fig. 2 Simplified three-dimensional model of the bridge

Table 2 Material properties of concrete and steel

Concrete material	
Compressive strength	35 MPa
Tensile strength	3.5 MPa
Crushing strain	0.002
Steel material	
Elastic modulus	200 GPa
Yielding strength (reinforcing steel)	400 MPa
Yielding strength (tendon)	1860 MPa
Strain hardening	0.001

Table 3 Percent reduction in stiffness of each member

Member	Damage grade	Damage index	Percent reduction in stiffness
30th pier	B	0.1	10%
31st pier	C	0.3	30%
32nd pier	C	0.3	30%
30th girder (end)	C	0.3	30%
30th girder (center)	B	0.1	10%
31st girder (end)	C	0.3	30%
31st girder (center)	B	0.1	10%

model has been validated in previous studies involving slab-on-girder bridges (Chan and Chan 1999), composite steel girder bridges (Chung and Sotelino 2005), and PSC girder bridges (Chung *et al*. 2005), with comparisons to experimental results.

The PSC box girder and RC piers were modeled using three-dimensional cubic elements, with the girder represented by a concrete rectangular box section and the piers by RC rectangular sections, as defined in Zeus-NL. The PSC tendons were rigidly connected to the box girder, and a pretension force was applied to simulate the prestressing effect. A joint element was used to model the interaction between the girder and the piers, while equivalent spring elements were assigned at each end of the model to simulate boundary conditions (Wilson and Tan 1990). In the piers, vertical reinforcement was modeled using 29 mm diameter bars spaced at 150 mm intervals. Material properties for concrete and steel in the intact bridge are summarized in Table 2. To model the deteriorated condition, a damage index representing a percentage reduction in elastic modulus was applied, as demonstrated in previous research (Yoon *et al*. 2022b). In the previous research, Barroso and Rodriguez (2004) proposed representing structural damage as a reduction in elastic modulus. Similarly, Zimmerman and Kauk (1994) evaluated damage indicators based on stiffness changes, and Pandey and Biswas (1994) used the inverse stiffness matrix to identify structural damage. Furthermore, several studies have developed and experimentally validated damage indices based on elastic modulus reduction (Cha and Buyukozturk 2015, Duque 2017, Tan *et al*. 2017). Accordingly, the percent reduction in elastic modulus is assumed to equal the damage index, and the FE model is updated to reflect the current structural condition. Table 3 presents the stiffness reduction ratios for individual members. Material nonlinearities for both concrete and reinforcing steel were incorporated into the model.

Fig. 3 illustrates the mode shapes and corresponding natural frequencies of the first three vibration modes of the deteriorated bridge. The x-, y-, and z-axes represent the longitudinal, vertical, and lateral directions, respectively. The first three modes were observed in two lateral directions and one vertical direction, with no dominant mode identified in the longitudinal direction. The natural frequencies obtained from the FE model fall within a reasonable range when compared with those of similar bridges in terms of span length and girder width (Li *et al*. 2014b, Vicente *et al*. 2015).

3.3 Nonlinear time-history analysis

To derive the aftershock fragility curves, nonlinear time-history analyses were performed using the developed FE model. To address the uncertainty inherent in earthquake ground motions, ten sets of mainshock–aftershock sequential ground motions were selected, with both horizontal components applied simultaneously. As vertical ground motions typically exhibit significantly lower amplitudes than horizontal components, vertical acceleration was excluded from the analysis.

Table 4 lists the selected input ground motions, which were obtained from the Pacific Earthquake Engineering Research Center (PEER) NGA database (Ancheta *et al*. 2014). The NGA-West2 database primarily includes records from active tectonic regions, such as California, dominated by shallow crustal earthquakes. In contrast, earthquakes on the Korean Peninsula are generally short in duration and high in frequency, with small- to moderate magnitudes. Nevertheless, the selected records adequately capture the key characteristics of mainshock–aftershock sequences required to evaluate cumulative seismic demands on the

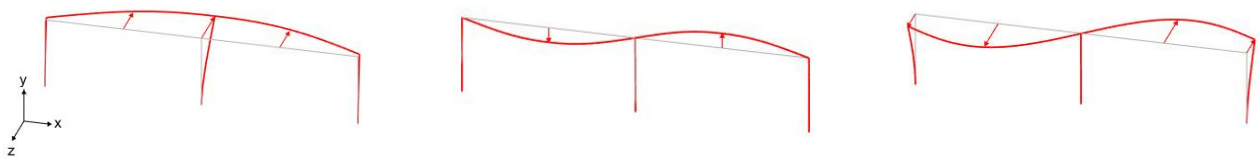

(a) Mode 1: 2.70 Hz (lateral) (b) Mode 2: 4.41 Hz (vertical) (c) Mode 3: 4.81 Hz (lateral)

Fig. 3 Mode shapes of the bridge

Table 4 Selected mainshock-aftershock sequences

No.	Event	Station	Type	M_w	PGA (g)	Record name
1	1983 Coalinga	Pleasant Valley P.P. - yard	Mainshock	6.36	0.6024	RSN368_COALINGA.H_H-PVY045.AT2
			Aftershock	5.09	0.0986	RSN383_COALINGA_A-PVY045.AT2
			Mainshock	6.36	0.5254	RSN368_COALINGA.H_H-PVY135.AT2
			Aftershock	5.09	0.2107	RSN383_COALINGA_A-PVY135.AT2
2	1979 Imperial Valley	El Centro Array #11	Mainshock	6.53	0.3668	RSN174_IMPVALL.H_H-E11140.AT2
			Aftershock	5.01	0.0972	RSN199_IMPVALL.A_A-E11140.AT2
			Mainshock	6.53	0.3794	RSN174_IMPVALL.H_H-E11230.AT2
			Aftershock	5.01	0.1924	RSN199_IMPVALL.A_A-E11230.AT2
3	1980 Livermore	San Ramon fire station	Mainshock	5.8	0.0551	RSN215_LIVERMOR_A-SRM070.AT2
			Aftershock	5.42	0.0455	RSN224_LIVERMOR_B-SRM070.AT2
			Mainshock	5.8	0.0365	RSN215_LIVERMOR_A-SRM340.AT2
			Aftershock	5.42	0.0540	RSN224_LIVERMOR_B-SRM340.AT2
4	1980 Mammoth Lakes	Long Valley Dam (Upr L Abut)	Mainshock	6.06	0.4303	RSN231_MAMMOTH.I_I-LUL000.AT2
			Aftershock	5.69	0.1933	RSN234_MAMMOTH.J_J-LUL000.AT2
			Mainshock	6.06	0.2713	RSN231_MAMMOTH.I_I-LUL090.AT2
			Aftershock	5.69	0.0660	RSN234_MAMMOTH.J_J-LUL090.AT2
5	1994 Northridge	Castaic-old ridge route	Mainshock	6.69	0.5683	RSN963_NORTHR_ORR090.AT2
			Aftershock	5.93	0.1384	RSN1676_NORTH142_ORR090.AT2
			Mainshock	6.69	0.5142	RSN963_NORTHR_ORR360.AT2
			Aftershock	5.93	0.1189	RSN1676_NORTH142_ORR360.AT2
6	1994 Northridge	Moorpark fire station	Mainshock	6.69	0.1931	RSN1039_NORTHR_MRP090.AT2
			Aftershock	5.93	0.1395	RSN1681_NORTH142_MRP090.AT2
			Mainshock	6.69	0.2918	RSN1039_NORTHR_MRP180.AT2
			Aftershock	5.93	0.1843	RSN1681_NORTH142_MRP180.AT2
7	1987 Whittier Narrows	Downey-Birchdale	Mainshock	5.99	0.2317	RSN614_WHITTIER.A_A-BIR090.AT2
			Aftershock	5.27	0.1604	RSN3701_WHITTIER.B_B-BIR090.AT2
			Mainshock	5.99	0.3482	RSN614_WHITTIER.A_A-BIR180.AT2
			Aftershock	5.27	0.1284	RSN3701_WHITTIER.B_B-BIR180.AT2
8	1986 Kalamata	Kalamata (bsmt)	Mainshock	6.2	0.2386	RSN564_GREECE_H-KAL-NS.AT2
			Aftershock	5.4	0.2414	RSN565_GREECE_J-KAL-NS.AT2
			Mainshock	6.2	0.2724	RSN564_GREECE_H-KAL-WE.AT2
			Aftershock	5.4	0.1419	RSN565_GREECE_J-KAL-WE.AT2
9	1976 Friuli	Tolmezzo	Mainshock	6.5	0.3571	RSN125_FRIULI.A_A-TMZ000.AT2
			Aftershock	5.2	0.1174	RSN4267_FRIULI.P_C-TMZ000.AT2
			Mainshock	6.5	0.3151	RSN125_FRIULI.A_A-TMZ270.AT2
			Aftershock	5.2	0.0729	RSN4267_FRIULI.P_C-TMZ090.AT2
10	1986 Chalfant	Zack Brothers Ranch	Mainshock	6.19	0.4472	RSN558_CHALFANT.A_A-ZAK270.AT2
			Aftershock	5.65	0.1643	RSN561_CHALFANT.B_C-ZAK270.AT2
			Mainshock	6.19	0.4005	RSN558_CHALFANT.A_A-ZAK360.AT2
			Aftershock	5.65	0.1133	RSN561_CHALFANT.B_C-ZAK360.AT2

target bridge. Fig. 4 presents the acceleration response spectra with 5% damping for the selected ground motions in both longitudinal and lateral directions. PGA was chosen as the IM, and the input motions were scaled from 0.1 g to 1.0 g PGA in 0.1 g increments to enable a comprehensive evaluation of structural response. Scaling was based on the PGA of the mainshock ground motions, and the same scaling factors were applied to their corresponding aftershock ground motions.

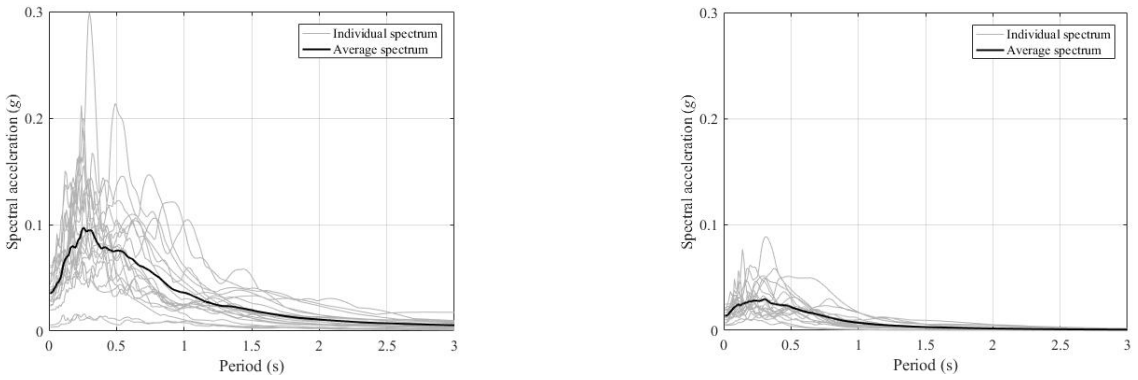

(a) Mainshock (b) Aftershock

Fig. 4 Response spectrum

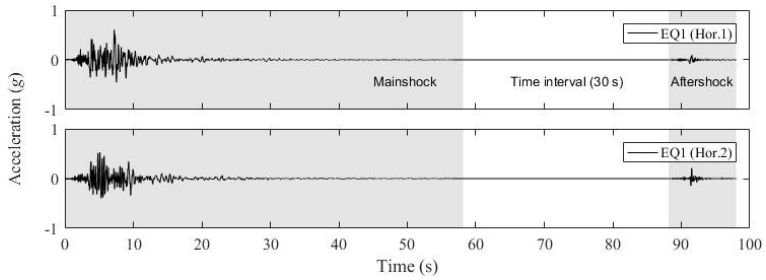

Fig. 5 Example of mainshock-aftershock sequential ground motions

To generate input ground motions representing mainshock–aftershock sequences, a 30-second interval of zero acceleration was inserted between the mainshock and aftershock acceleration time histories. This approach allows the structure to return to a quasi-static state before the onset of the aftershock, as recommended in previous studies (Hu *et al*. 2021, Di Sarno and Pugliese 2021). The constructed sequential ground motions are illustrated in Fig. 5.

This study adopted the drift ratio defined as the lateral displacement normalized by pier height, as the primary measure to quantify seismic demand. Through nonlinear time-history analyses, the maximum drift ratios under aftershock excitation were collected for each pier at various PGA levels. Fig. 6 presents the drift ratio time histories under both mainshock–aftershock sequences and single aftershock events. As shown in Fig. 6(a), complete drift ratio histories were successfully recorded over the entire duration of the mainshock–aftershock sequences. However, in some cases (e.g., Fig. 6(b)), unstable structural responses were observed before the aftershock excitation commenced. Since the objective of this study is to derive aftershock fragility curves, such instances were excluded from the derivation of the PSDM for the mainshock–aftershock sequences.

Using pairs of maximum drift ratios and corresponding PGA values, regression analyses were performed in the natural logarithmic space for each pier and each earthquake excitation type (i.e., mainshock–aftershock sequence and aftershock only) to develop the PSDMs. Fig. 7 illustrates the resulting PSDMs for each pier under the two excitation types, while the corresponding model parameters are summarized in Table 5. Although the 31st and 32nd piers exhibited more severe damage grades than the 30th pier, the seismic responses of the 30th and 32nd piers had limited influence on overall demand due to the boundary conditions in the FE model. Note that both ends were constrained by equivalent spring elements. Therefore, this study focused on the seismic fragility of the 31st pier, where relatively higher drift ratios were observed. The logarithmic dispersion of seismic demand, $\beta_{D|IM}$, for the 31st pier was calculated using Eq. (4), and the results are presented in Table 6.

When comparing the seismic demands between the mainshock–aftershock sequence and the single aftershock,

Table 5 Parameters of PSDMSs for each pier

Pier	Type	PSDM
30th pier	Sequence	$D = 0.0014 \times IM^{0.3012}$
	Aftershock	$D = 0.0010 \times IM^{1.0673}$
31st pier	Sequence	$D = 0.0080 \times IM^{0.4513}$
	Aftershock	$D = 0.0048 \times IM^{1.1958}$
32nd pier	Sequence	$D = 0.0015 \times IM^{0.3554}$
	Aftershock	$D = 0.0011 \times IM^{1.5080}$

Table 6 Logarithmic dispersion of seismic demand

EQ	$\beta_{D\|IM}$		
	30th pier	31st pier	32nd pier
Sequence	0.6172	0.9026	0.6133
Aftershock	0.9082	1.1841	0.8944

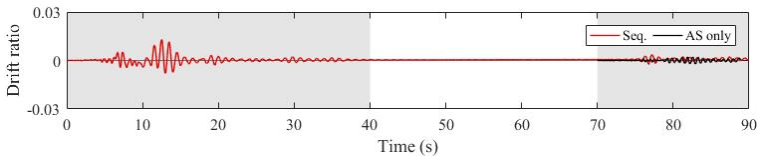

(a) EQ5 (0.9 g PGA)

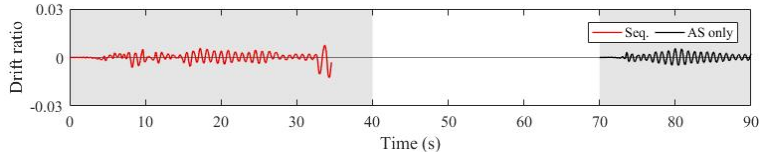

(b) EQ6 (0.9 g PGA)

Fig. 6 Drift ratio time-history

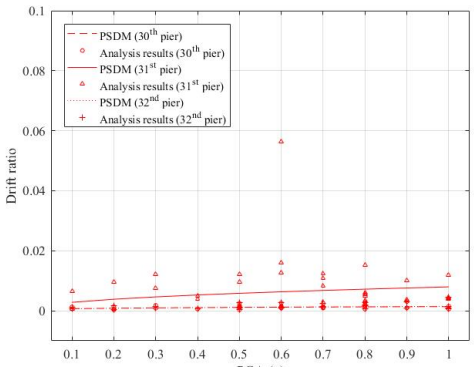

(a) Mainshock-aftershock sequence

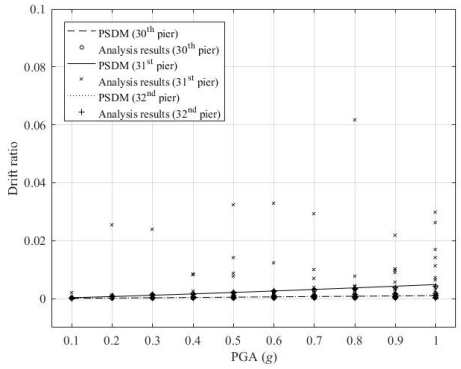

(b) Single aftershock

Fig. 7 PSDMs for each pier

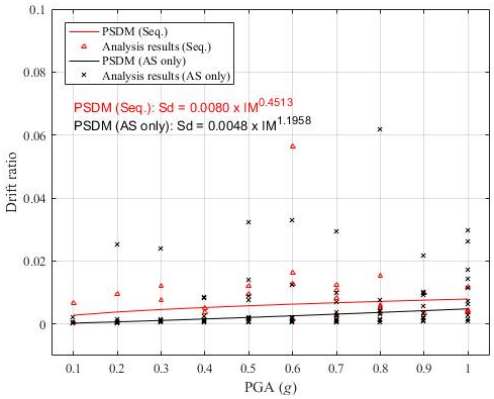

Fig. 8 Comparison of PSDMs for the 31st pier under mainshock-aftershock sequence and single aftershock

it was observed that the demand resulting from the sequence was consistently higher. Fig. 8 presents a comparison of the PSDMs for the 31st pier, illustrating that the pier subjected to the mainshock–aftershock sequence exhibits a relatively greater seismic demand compared to the case with only a single aftershock.

3.4 Aftershock fragility curve derivation

To derive the aftershock fragility curves, five damage states were considered: no damage, slight, moderate, extensive, and complete damage. The drift limits corresponding to each damage state were adopted from the recommendations by Dutta and Mander (1998), as listed in Table 7. The proposed modeling approach incorporates deterioration, ensuring that adjusted structural response realistically represents the behavior of deteriorated PSC bridges, while maintaining the original capacity limits (Yoon *et al*. 2022a). The logarithmic dispersion of structural capacity, β_C, was assumed to be 0.35 for all damage states, following the commonly accepted values for seismic fragility assessments of bridges (Ramanathan *et al*. 2015, Ghosh and Sood 2016).

Table 7 Drift limits for each damage state (Dutta and Mander 1998)

Damage state	Description	Drift limit (for non-seismically design)
Almost No	First yield	0.005
Slight	Cracking, spalling	0.007
Moderate	Loss of anchorage	0.015
Extensive	Incipient column collapse	0.025
Complete	Column collapse	0.005

Using Eq. (5), seismic fragility curves were derived for each damage state, as shown in Fig. 9. In addition, the fragility curves of the mainshock–aftershock sequence were

Table 8 Failure probabilities of the 31st pier

Damage state	Type	0.1 *g*	0.2 *g*	0.3 *g*	0.4 *g*	0.5 *g*	0.6 *g*	0.7 *g*	0.8 *g*	0.9 *g*	1.0 *g*
Almost No	Sequence	0.277	0.394	0.468	0.521	0.563	0.596	0.623	0.647	0.667	0.685
	Aftershock	0.012	0.057	0.117	0.181	0.243	0.301	0.355	0.404	0.449	0.490
Slight	Sequence	0.173	0.268	0.334	0.384	0.425	0.458	0.487	0.512	0.533	0.553
	Aftershock	0.006	0.032	0.072	0.118	0.166	0.214	0.260	0.303	0.344	0.383
Moderate	Sequence	0.042	0.080	0.112	0.140	0.164	0.186	0.206	0.224	0.241	0.256
	Aftershock	0.001	0.007	0.019	0.036	0.056	0.079	0.104	0.129	0.154	0.180
Extensive	Sequence	0.012	0.027	0.041	0.054	0.066	0.078	0.089	0.099	0.109	0.119
	Aftershock	0.000	0.002	0.006	0.013	0.023	0.034	0.047	0.061	0.076	0.092
Complete	Sequence	0.001	0.004	0.007	0.010	0.013	0.016	0.019	0.023	0.026	0.029
	Aftershock	0.000	0.000	0.001	0.003	0.005	0.009	0.013	0.018	0.023	0.029

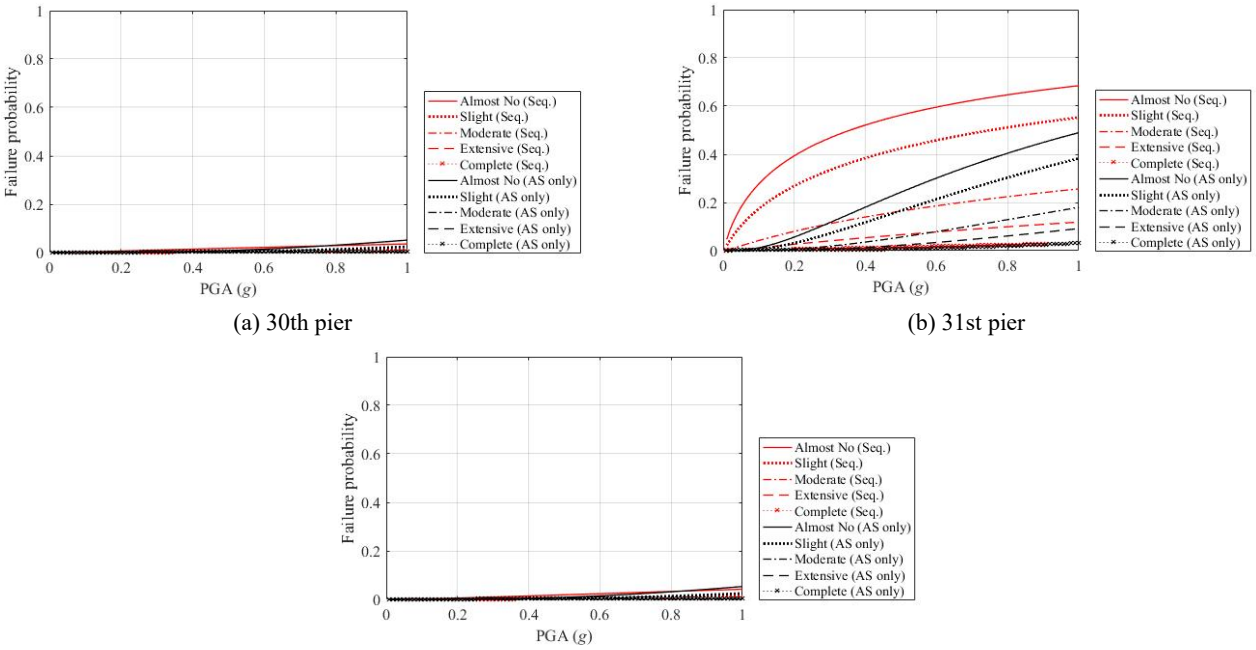

(a) 30th pier

(b) 31st pier

(c) 32nd piert

Fig. 9 Aftershock fragility curves

compared with those of a single aftershock. As a result, failure probabilities of the 30th and 32nd piers were much lower than the 31st pier, which results from the boundary condition as mentioned above. Focusing on the 31st pier, it was found that failure probabilities under the mainshock–aftershock sequence were overall higher due to the structural deformation caused by the mainshock preceding the aftershock when compared to those under single aftershocks. The maximum difference in failure probabilities between the mainshock–aftershock sequence and the single aftershock scenarios was 35.1% at 0.3 g PGA, which occurred at the Almost No damage state as presented in Table 8. As the level of damage increased, the difference in failure probabilities tended to decrease.

4. Conclusions

The objective of this study was to investigate the impact of mainshock–aftershock sequences on the aftershock fragility of a deteriorated PSC bridge. To achieve this, aftershock fragility curves were derived for both mainshock–aftershock sequential ground motions and single aftershock ground motions, and the results were compared. For the seismic fragility assessment, a conventional method using a simple probability distribution function was applied, with failure probabilities calculated under the assumption that both seismic demand and capacity follow lognormal distributions. The drift ratio of the pier was adopted as the measure of seismic demand, and the threshold values for the selected damage states, as recommended in previous studies, were utilized.

In this numerical example, the Deungsun Bridge,

approximately 40 years old and located in South Korea, was selected as the target structure. Structural deterioration was found to influence seismic capacity, and the extent of deterioration in the target bridge was assessed using a novel approach based on UAV-based damage detection. Nonlinear time-history analyses were performed with varying ground motion intensities, considering ten sets of mainshock–aftershock sequences to account for the uncertainty of ground motions. For comparison, nonlinear structural responses were also computed for single aftershock ground motions. It was found that the seismic demand at the middle pier (i.e., the 31st pier) was greater than at the other piers, leading to a focus on the 31st pier for aftershock fragility analysis. The results of the aftershock fragility assessment indicated that failure probabilities under the mainshock–aftershock sequence increased due to the structural deformation caused by the mainshock preceding the aftershock. Moreover, the difference in failure probabilities between the mainshock–aftershock sequence and the single aftershock scenario tended to decrease as the damage level increased.

Acknowledgments

This work was supported by the National Research Foundation of Korea(NRF) grant funded by the Korea government (MSIT) (No. RS-2024-00415881).

References

Akin, O. and Sahin, M. (2017), "Active neuro-adaptive vibration suppression of a smart beam", *Smart Struct. Syst., Int. J.*, **20**(6), 657-668. https://doi.org/10.12989/sss.2017.20.6.657

Ancheta, T.D., Darragh, R.B., Stewart, J.P., Seyhan, E., Silva, W.J., Chiou, B.S.J., Wooddell, K.E., Graves, R.W., Kottke, A.R., Boore, D.M. and Kishida, T. (2014), "NGA-West2 database", *Earthq. Spectra*, **30**(3), 989-1005. https://doi.org/10.1193/070913EQS197M

Barroso, L.R. and Rodriguez, R. (2004), "Damage detection utilizing the damage index method to a benchmark structure", *J. Eng. Mech.*, **130**(2), 142-151. https://doi.org/10.1061/(ASCE)0733-9399(2004)130:2(142)

Cha, Y.J. and Buyukozturk, O. (2015), "Structural damage detection using modal strain energy and hybrid multiobjective optimization", *Comput.-Aided Civil Infrastr. Eng.*, **30**(5), 347-358. https://doi.org/10.1111/mice.12122

Chan, T.H. and Chan, J.H. (1999), "The use of eccentric beam elements in the analysis of slab-on-girder bridges", *Struct. Eng. Mech., Int. J.*, **8**(1), 85-102. https://doi.org/10.12989/sem.1999.8.1.085

Choi, E., DesRoches, R. and Nielson, B. (2004), "Seismic fragility of typical bridges in moderate seismic zones", *Eng. Struct.*, **26**(2), 187-199. https://doi.org/10.1016/j.engstruct.2003.09.006

Chung, W. and Sotelino, E.D. (2005), "Nonlinear finite-element analysis of composite steel girder bridges", *J. Struct. Eng.*, **131**(2), 304-313. https://doi.org/10.1061/(ASCE)0733-9445(2005)131:2(304)

Chung, W., Phuvoravan, K., Liu, J. and Sotelino, E.D. (2005), "Applicabiliy of the simplified load distribution factor equation to PSC girder bridges", *KSCE J. Civil Eng.*, **9**(4), 313-319. https://doi.org/10.1007/BF02829044

Cornell, C.A., Jalayer, F., Hamburger, R.O. and Foutch, D.A. (2002), "Probabilistic basis for 2000 SAC federal emergency management agency steel moment frame guidelines", *J. Struct. Eng.*, **128**(4), 526-533. https://doi.org/10.1061/(ASCE)0733-9445(2002)128:4(526)

Di Sarno, L. and Pugliese, F. (2021), "Effects of mainshock-aftershock sequences on fragility analysis of RC buildings with ageing", *Eng. Struct.*, **232**, p. 111837. https://doi.org/10.1016/j.engstruct.2020.111837

Duque, L. (2017), "UAV-based bridge inspection and computational simulations", South Dakota State University. https://openprairie.sdstate.edu/etd/2159

Dutta, A. and Mander, J.B. (1998), "Seismic fragility analysis of highway bridges", INCEDE-MCEER Center-to-Center Project Workshop on Earthquake Engineering Frontiers in Transportation Systems, Tokyo, June.

Elnashai, A., Papanikolaou, V. and Lee, D. (2010), "Zeus-NL-A system for inelastic analysis of structures-user manual", Mid-America Earthquake (MAE) Center, Department of Civil and Environmental Engineering, University of Illinois at Urbana-Champaign, Urbana, IL, USA.

Gaetani d'Aragona, M., Polese, M., Elwood, K.J., Baradaran Shoraka, M. and Prota, A. (2017), "Aftershock collapse fragility curves for non-ductile RC buildings: a scenario-based assessment", *Earthq. Eng. Struct. Dyn.*, **46**(13), 2083-2102. https://doi.org/10.1002/eqe.2894

Ghosh, J. and Sood, P. (2016), "Consideration of time-evolving capacity distributions and improved degradation models for seismic fragility assessment of aging highway bridges", *Reliabil. Eng. Syst. Safety*, **154**, 197-218. https://doi.org/10.1016/j.ress.2016.06.001

Hakim, S. and Razak, H.A. (2014), "Modal parameters based structural damage detection using artificial neural networks-a review", *Smart Struct. Syst., Int. J.*, **14**(2), 159-189. https://doi.org/10.12989/sss.2014.14.2.159

He, K., Gkioxari, G., Dollár, P. and Girshick, R. (2017), "Mask r-cnn", *Proceedings of the IEEE International Conference on Computer Vision*, Santiago, Chile, December.

Hu, S., Wang, W. and Shahria Alam, M. (2021), "Comparative study on seismic fragility assessment of self-centering energy-absorbing dual rocking core versus buckling restrained braced systems under mainshock–aftershock sequences", *J. Struct. Eng.*, **147**(9), p. 04021124. https://doi.org/10.1061/(ASCE)ST.1943-541X.0003082

KMA (2017), Seismological Annual Report 2016; Korea Meteorological Administration, Seoul, Republic of Korea. https://www.kma.go.kr/download_01/earthquake/earthquake_2016.pdf [In Korean]

Lee, Y.-J. and Moon, D.-S. (2014), "A new methodology of the development of seismic fragility curves", *Smart Struct. Syst., Int. J.*, **14**(5), 847-867. https://doi.org/10.12989/sss.2014.14.5.847

Lee, S., Kim, B. and Lee, Y.-J. (2019), "Seismic Fragility Analysis of Steel Liquid Storage Tanks Using Earthquake Ground Motions Recorded in Korea", *Mathe. Probl. Eng.*, **2019**, p. 6190159. https://doi.org/10.1155/2019/6190159

Lee, S., Moon, D.-S., Kim, B., Kim, J. and Lee, Y.-J. (2021), "Hybrid fragility curve derivation of buildings based on post-earthquake reconnaissance data", *Smart Struct. Syst., Int. J.*, **28**(4), 553-566. https://doi.org/10.12989/sss.2021.28.4.553

Li, Y., Song, R. and Van De Lindt, J.W. (2014a), "Collapse fragility of steel structures subjected to earthquake mainshock-aftershock sequences", *J. Struct. Eng.*, **140**(12), p. 04014095. https://doi.org/10.1061/(ASCE)ST.1943-541X.0001019

Li, P.-F., Wang, Y.-F., Liu, B.-D. and Su, L. (2014b), "Damping properties of highway bridges in China", *J. Bridge Eng.*, **19**(5), p. 04014005. https://doi.org/10.1061/(ASCE)BE.1943-5592.0000578

Mackie, K.R. and Stojadinović, B. (2005), "Comparison of incremental dynamic, cloud, and stripe methods for computing probabilistic seismic demand models", In: *Structures Congress 2005*: *Metropolis and Beyond*, New York, USA, April.

Mangalathu, S., Choi, E., Park, H.C. and Jeon, J.-S. (2018), "Probabilistic seismic vulnerability assessment of tall horizontally curved concrete bridges in California", *J. Perform. Constr. Facil.*, **32**(6), p. 04018080. https://doi.org/10.1061/(ASCE)CF.1943-5509.0001231

MOLIT (2019), Detail Guidelines for Safety Inspections and Full Safety Examinations, Ministry of Land Infrastructure and Transport, Korea Authority of Land and Infrastructure Safety.

MOLIT (2020), Special act on the Safety and Maintenance of Facilities, Ministry of Land Infrastructure and Transport.

Moon, D.-S., Lee, Y.-J. and Lee, S. (2018), "Fragility analysis of space reinforced concrete frame structures with structural irregularity in plan", *J. Struct. Eng.*, **144**(8), p. 04018096. https://doi.org/10.1061/(ASCE)ST.1943-541X.0002092

Nielson, B.G. and DesRoches, R. (2007), "Analytical seismic fragility curves for typical bridges in the central and southeastern United States", *Earthq. Spectra*, **23**(3), 615-633. https://doi.org/10.1193/1.2756815

Oh, B.-H., Shin, K.-J., Kim, K.-S., Kim, J.-S. and Lee, S.-C. (2001), "Improved Criteria for Condition Assessment of Bridges Based on Visual Inspection", *J. Korea Inst. Struct. Maint. Inspect.*, **5**(4), 205-213. [In Korean]

Omranian, E., Abdelnaby, A.E. and Abdollahzadeh, G. (2018), "Seismic vulnerability assessment of RC skew bridges subjected to mainshock-aftershock sequences", *Soil Dyn. Earthq. Eng.*, **114**, 186-197. https://doi.org/10.1016/j.soildyn.2018.07.007

Onat, O. and Gul, M. (2018), "Application of artificial neural networks to the prediction of out-of-plane response of infill walls subjected to shake table", *Smart Struct. Syst., Int. J.*, **21**(4), 521-535. https://doi.org/10.12989/sss.2018.21.4.521

Padgett, J.E. and DesRoches, R. (2008), "Methodology for the development of analytical fragility curves for retrofitted bridges", *Earthq. Eng. Struct. Dyn.*, **37**(8), 1157-1174. https://doi.org/10.1002/eqe.801

Pandey, A.K. and Biswas, M. (1994), "Damage detection in structures using changes in flexibility", *J. Sound Vib.*, **169**(1), 3-17. https://doi.org/10.1006/jsvi.1994.1002

Pang, R., Xu, B., Zhang, X., Zhou, Y. and Kong, X. (2019), "Seismic performance investigation of high CFRDs subjected to mainshock-aftershock sequences", *Soil Dyn. Earthq. Eng.*, **116**, 82-85. https://doi.org/10.1016/j.soildyn.2018.09.049

Peng-hui, L., Hong-ping, Z., Hui, L. and Shun, W. (2015), "Structural damage identification based on genetically trained ANNs in beams", *Smart Struct. Syst., Int. J.*, **15**(1), 227-244. https://doi.org/10.12989/sss.2015.15.1.227

Rajeev, P. and Tesfamariam, S. (2012), "Seismic fragilities for reinforced concrete buildings with consideration of irregularities", *Struct. Safety*, **39**, 1-13. https://doi.org/10.1016/j.strusafe.2012.06.001

Ramanathan, K., Padgett, J.E. and DesRoches, R. (2015), "Temporal evolution of seismic fragility curves for concrete box-girder bridges in California", *Eng. Struct.*, **97**, 29-46. https://doi.org/10.1016/j.engstruct.2015.03.069

Shinozuka, M., Feng, M., Kim, H., Uzawa, T. and Ueda, T. (2003), "Statistical analysis of fragility curves", Technical Report MCEER-03-002.

Tan, Z.X., Thambiratnam, D.P., Chan, T.H.T. and Razak, H.A. (2017), "Detecting damage in steel beams using modal strain energy based damage index and Artificial Neural Network", *Eng. Fail. Anal.*, **79**, 253-262. https://doi.org/10.1016/j.engfailanal.2017.04.035

Vicente, M.A., González, D.C. and Fu, G. (2015), "Static and dynamic testing of high-speed rail bridges in Spain", *J. Bridge Eng.*, **20**(2), p. 06014006. https://doi.org/10.1061/(ASCE)BE.1943-5592.0000654

Wilson, J.C. and Tan, B.S. (1990), "Bridge abutments: formulation of simple model for earthquake response analysis", *J. Eng. Mech.*, **116**(8), 1828-1837. https://doi.org/10.1061/(ASCE)0733-9399(1990)116:8(1828)

Yoon, S., Lee, Y.-J. and Jung, H.-J. (2018), "A comprehensive framework for seismic risk assessment of urban water transmission networks", *Int. J. Disaster Risk Reduct.*, **31**, 983-994. https://doi.org/10.1016/j.ijdrr.2018.09.002

Yoon, S., Lee, Y.-J. and Jung, H.-J. (2020a), "A comprehensive approach to flow-based seismic risk analysis of water transmission network", *Struct. Eng. Mech., Int. J.*, **73**(3), 339-351. https://doi.org/10.12989/sem.2020.73.3.339

Yoon, S., Lee, Y.-J. and Jung, H.-J. (2020b), "Accelerated Monte Carlo analysis of flow-based system reliability through artificial neural network-based surrogate models", *Smart Struct. Syst., Int. J.*, **26**(2), 175-184. https://doi.org/10.12989/sss.2020.26.2.175

Yoon, S., Lee, Y.-J. and Jung, H.-J. (2021a), "Flow-based seismic resilience assessment of urban water transmission network", *Struct. Eng. Mech., Int. J.*, **79**(4), 517-529. https://doi.org/10.12989/sem.2021.79.4.517

Yoon, S., Gwon, G.-H., Lee, J.-H. and Jung, H.-J. (2021b), "Three-dimensional image coordinate-based missing region of interest area detection and damage localization for bridge visual inspection using unmanned aerial vehicles", *Struct. Health Monitor.*, **20**(4), 1462-1475. https://doi.org/10.1177/1475921720918675

Yoon, S., Lee, S., Kye, S., Kim, I.H., Jung, H.J. and Spencer Jr, B.F. (2022a), "Seismic fragility analysis of deteriorated bridge structures employing a UAV inspection-based updated digital twin", *Struct. Multidiscipl. Optimiz.*, **65**(12), p. 346. https://doi.org/10.1007/s00158-022-03445-0

Yoon, S., Spencer Jr, B.F., Lee, S., Jung, H.J. and Kim, I.H. (2022b), "A novel approach to assess the seismic performance of deteriorated bridge structures by employing UAV-based damage detection", *Struct. Control Health Monitor.*, **29**(7), p. e2964. https://doi.org/10.1002/stc.2964

Zhang, J. and Zirakian, T. (2015), "Probabilistic assessment of structures with SPSW systems and LYP steel infill plates using fragility function method", *Eng. Struct.*, **85**, 195-205. https://doi.org/10.1016/j.engstruct.2014.12.027

Zhang, H., Sun, T., Hou, S.W., Gao, Q.M. and Li, X. (2021), "Effect of aftershocks on seismic fragilities of single-story masonry structures", *Front. Phys.*, **9**, p. 695111. https://doi.org/10.3389/fphy.2021.695111

Zimmerman, D.C. and Kauk, M. (1994), "Structural damage detection using a minimum rank update theory", *J. Vib. Acoustic*, **116**(2), 221-231. https://doi.org/10.1115/1.2930416